Nigerian Journal of Technology (NIJOTECH)
Vol. 44, No. 2, June, 2025, pp.273 - 281
www.nijotech.com

Print ISSN: 0331-8443
Electronic ISSN: 2467-8821
https://doi.org/10.4314/njt.v44i2.11

SURROGATE-MODEL-BASED OPTIMIZATION DESIGN OF WOUND-FIELD FLUX SWITCHING MACHINE FOR INDUSTRIAL APPLICATIONS

AUTHORS:
C. E. Abunike[1,*], U. B. Akuru[2], O. I. Okoro[3], C. C. Awah[4], I. E. Nkan[5], U. O. Innocent[6], E. E. Okpo[7], P. I. Udenze[8], and M. J. Mbunwe[9]

AFFILIATIONS:
[1,3,4]Department of Electrical/Electronic Engineering, Michael Okpara University of Agriculture, Umudike, Nigeria
[2]Department of Electrical Engineering, Tshwane University of Technology, Pretoria, South Africa.
[5,7]Department of Electrical/Electronic Engineering, Akwa Ibom State University, Ikot Akpaden, Nigeria.
[6]Department of Electrical/Electronic Engineering, Alex-Ekwueme Federal University, Ndufu-Alike, Nigeria
[8]Department of Electrical/Electronic Engineering, University of Agriculture, Makurdi, Nigeria
[9]Department of Electrical Engineering, University of Nigeria, Nsukka, Nigeria

***CORRESPONDING AUTHOR:**
Email: abunike.emmanuel@mouau.edu.ng

ARTICLE HISTORY:
Received: 04 April, 2025.
Revised: 09 June, 2025.
Accepted: 17 June, 2025.
Published: 07 July, 2025.

KEYWORDS:
Finite Element Analysis, Response Surface Methodology, Surrogate Model, Torque Optimization, Torque Ripple Minimization, Wound-Field Flux Switching Machine.

ARTICLE INCLUDES:
Peer review

DATA AVAILABILITY:
On request from author(s)

EDITORS:
Ozoemena Anthony Ani

FUNDING:
TETFUND National Research Grant Intervention

Abstract
The Wound-Field Flux Switching Machine (WFFSM) is a promising solution for high-performance industrial applications, offering high torque density, brushless operation, and controllable excitation flux. However, optimizing its design is challenging due to nonlinear flux interactions and multiple competing objectives. This study presents a surrogate-model-based optimization framework using response surface methodology (RSM) and multi-objective genetic algorithm (MOGA) to enhance the electromagnetic performance of a 1.5 kW WFFSM. Finite element analysis (FEA)-driven sampling and RSM surrogate modeling enable efficient exploration of the design space. The optimized WFFSM achieves a 77.7% reduction in torque ripple compared to the initial model, along with significant improvements in torque output and enhanced back-EMF characteristics. The proposed approach contributes a novel, systematic optimization strategy specifically tailored for industrial WFFSM applications, ensuring improved efficiency, reliability, and adaptability in next-generation electric machines.

1.0 INTRODUCTION
The increasing demand for high-performance, energy-efficient, and cost-effective electric machines in industrial applications has driven significant advancements in the design and optimization of electric motors [1]. Wound Field Flux Switching Machines (WFFSMs) have emerged as a promising candidate due to their robust structure, high torque density, and excellent flux controllability. WFFSMs combine the advantages of both permanent magnet machines and switched reluctance machines, making them suitable for a wide range of industrial applications, including electric vehicles, renewable energy systems, and industrial automation [2-4]. However, the complex electromagnetic behavior and multi-objective design requirements of WFFSMs pose significant challenges in their optimization, necessitating the development of advanced design methodologies.

Traditional design optimization approaches for electric machines often rely on iterative trial-and-error methods, which are time-consuming and computationally expensive [5, 6]. In recent years, surrogate-model-based optimization techniques have received growing attention as an efficient alternative for the design of complex electromagnetic devices.

HOW TO CITE:
Abunike, C. E., Akuru, U. B., Okoro, O. I., Awah, C. C., Nkan, I. E., Innocent, U. O., Okpo, E. E., Udenze, P. I., and Mbunwe, M. J. "Surrogate-Model-Based Optimization Design of Wound-Field Flux Switching Machine for Industrial Applications", *Nigerian Journal of Technology*, 2025; 44(2), pp. 273 – 281; *https://doi.org/10.4314/njt.v44i2.11*

Surrogate models, also known as metamodels, approximate the behavior of high-fidelity simulations using data-driven techniques, enabling rapid evaluation of design candidates and reducing the computational burden. By integrating surrogate models with optimization algorithms, designers can efficiently explore the design space and identify optimal solutions that meet specific performance criteria [7, 8].

Recent studies have explored surrogate-model-based optimization for various electric machines, demonstrating improved efficiency, torque performance, and computational speed [7], [9], [10], [11]. In [9], a double-sided permanent magnet (PM)-excited flux-switching machine is optimized using a hybrid method combining gradient boosting decision trees and non-sorting genetic algorithm-II, leading to enhanced torque density. Similarly, [12] employs a hybrid surrogate model integrating Radial Basis Function (RBF) neural networks and support vector regression for optimizing a flux-modulated PM machine, significantly reducing harmonics and computational effort. In [13], a model-based multi-objective optimization method is applied to a hybrid-excitation switched flux machine, reducing optimization time from 67 hours to 2.3 hours while mitigating local flux saturation issues. A Kriging-based surrogate model is used in [14] for in-wheel hybrid-excitation flux-switching machine optimization, enhancing torque and efficiency while minimizing reliance on permanent magnets. Beyond electrical machines, [15] applies machine-learning-based surrogate modeling to optimize a multi-generation system, achieving superior performance across six conflicting objectives. Further, [16] introduces an adaptive surrogate-assisted optimization technique for an axial flux permanent magnet machine, leveraging local cascade ensemble learning to improve accuracy and computational efficiency. Additionally, emerging robust optimization strategies are being adopted for industrial electrical machines to address complex design trade-offs [17]. Lastly, [18] presents a machine-learning-assisted design for an interior permanent magnet synchronous motor, integrating fine and coarse mesh data to optimize performance while reducing simulation costs.

Despite these advancements, there remains a clear need for a comprehensive optimization framework specifically tailored to WFFSMs for industrial applications. Prior studies have often focused on isolated performance metrics, such as torque density or efficiency, without addressing the broader, system-level design requirements of industrial environments. Furthermore, the integration of surrogate models with advanced optimization algorithms, such as response surface-based algorithms or particle swarm optimization, has not been fully exploited for WFFSMs. Addressing this gap, the present study proposes a comprehensive surrogate-model-based multi-objective optimization framework for WFFSM design, which explicitly incorporates multiple performance objectives, practical industrial constraints, and manufacturability considerations. The framework is validated through high-fidelity finite element analysis (FEA), ensuring both accuracy and applicability to next-generation industrial electric machines.

2.0 MACHINE TOPOLOGY AND GEOMETRIC MODELING

The topology, sizing equations, and electromagnetic modeling of the WFFSM are presented in this section. The machine adopts a doubly salient structure, where both armature and field windings are housed within the stator, while the rotor remains passive. This design eliminates the need for permanent magnets, offering flexible flux control, making WFFSMs ideal for high-performance industrial applications.

The stator and rotor structures of the proposed WFFSM are illustrated in Figure 1. The stator features 24 slots, accommodating both armature and field windings, while the salient-pole rotor facilitates flux switching by modulating the magnetic path. The machine is rated at 1.5 kW, and both the stator and rotor cores are constructed from M400-50A electrical steel, ensuring high magnetic performance and reduced core losses.

The machine's sizing parameters are determined based on electromagnetic and mechanical constraints, ensuring optimal torque production, minimal losses, and manufacturability. The primary design variables are summarized in Table 1.

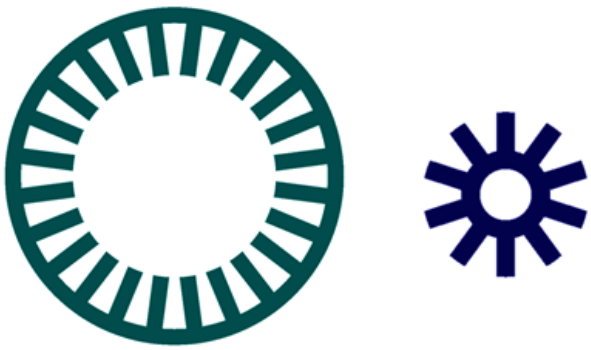

Figure 1: Stator and rotor structure of the proposed WFFSM

Table 1: Key parameters for the proposed WFFSM

Symbol	Parameter	Value
D_{out}	Stator outer diameter	186.98 mm
D_{in}	Stator inner diameter	112.19 mm
g	Airgap length	0.5 mm
l_s	Stack length	78.53 mm
N_s	Number of stator slots	24
N_r	Number of rotor poles	10
θ_s	Stator slot pitch	15^0
θ_r	Rotor pole pitch	36^0
N_{AC}	Number of armature turns	144 turns
N_{DC}	Number of field winding turns	144 turns

To ensure the WFFSM meets power and torque requirements, key sizing equations are employed. The stator outer diameter (D_{out}) is estimated based on the required output power (P_{out}), stator slot configuration, and magnetic loading [4]:

$$D_{out} = \left(\frac{4T_e N_s}{\sqrt{2}\pi^2 N_r k_f k_L \Lambda_0^3 A_e B_g \eta c_s} \right)^{1/3}, \quad (1)$$

where T_e, N_s, N_r, k_f, k_L, Λ, A_e, B_g, η, and c_s represent electromagnetic torque, number of stator slots, number of rotor poles, flux leakage factor, stack length ratio, electrical loading, peak airgap flux density, efficiency, and stator tooth arc factor, respectively.

The torque and power expressions are given in terms of rotor speed, ω_e, as:

$$T_e = \frac{P_{out}}{\omega_e}, \quad (2)$$

$$\omega_e = \frac{2\pi N_r}{60}, \quad (3)$$

and the aspect ratio is:

$$\Lambda_0 = \frac{D_{in}}{D_{out}}, \quad (4)$$

$$k_L = \frac{l_s}{D_{in}}. \quad (5)$$

Where D_{in} is the stator inner diameter, and l_s is the stack length. To achieve a balance between magnetic and electrical loading, the sum of the phase and field electrical loading is given as:

$$A_\Sigma = A_{AC} + A_{DC}, \quad (6)$$

Where A_{AC} and A_{DC} are the electrical loading of the armature and field windings, respectively.

This formulation ensures that flux density remains within practical operating limits, avoiding core saturation while maximizing performance.

3.0 SURROGATE-BASED OPTIMIZATION FRAMEWORK USING RESPONSE SURFACE METHODOLOGY

This section presents the mathematical formulation and computational framework for optimizing the WFFSM using Response Surface Methodology (RSM), as outlined in Figure 2. The optimization workflow follows a structured sequence of steps, starting with initialization of the WFFSM model, definition of the weights of the objective functions, parametric analysis, and finite element analysis (FEA) of the initial model, along with design of experiment (DOE)-based sampling to collect performance data. To enhance manufacturability and account for assembly tolerances, the air gap and stack length were modified during the parameterization process.

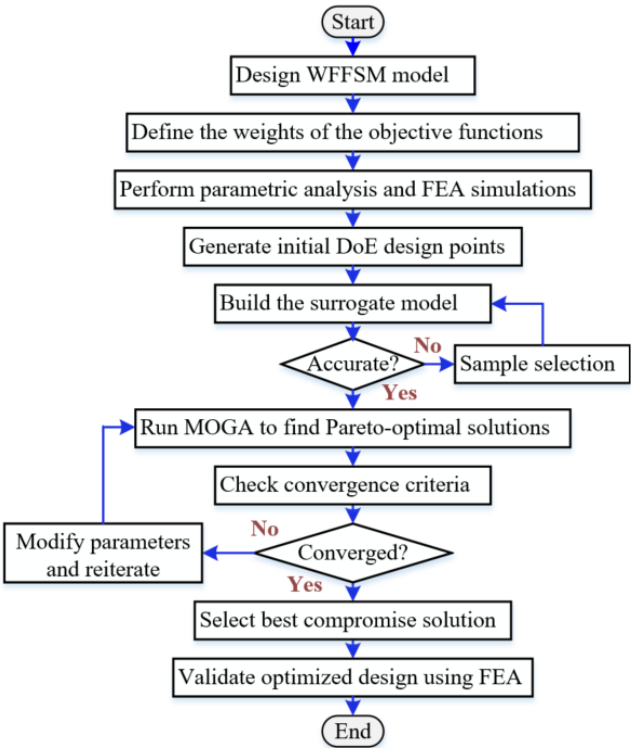

Figure 2: The proposed optimization flowchart for the WFFSM model

The air gap, initially 0.5 mm, was increased to 1.0 mm in the parameterized model to facilitate prototyping, as smaller air gaps can introduce fabrication challenges and misalignment issues. Likewise, the stack length was reduced from 78.53 mm in the initial model to 56 mm in the parameterized model, improving the torque-to-weight ratio, minimizing material usage, and enhancing manufacturability while maintaining performance. A response surface model is then constructed from the DoE dataset using regression techniques to approximate the relationship between design variables and performance objectives. The Multi-Objective Genetic Algorithm (MOGA) is employed to explore the design space and derive Pareto-optimal solutions. To ensure convergence, an iterative evaluation process is implemented, where the

optimization algorithm checks whether the solution has reached the desired criteria. If convergence is not achieved, the design parameters are modified, and the process is repeated until an optimal solution is obtained. Finally, the optimized WFFSM design undergoes high-fidelity FEA validation to confirm that the selected parameters achieve the desired electromagnetic performance within practical constraints. By systematically integrating these steps, the proposed methodology ensures an efficient, balanced, and computationally feasible optimization strategy for high-performance industrial applications.
To balance the competing objectives of maximizing average torque (T_{avg}) and minimizing torque ripple (ΔT_r), a weighted sum function is employed:

$$\min f(X) = w_1 f_1(X) + w_2 f_2(X), \quad (5)$$

where $f_1(X) = -T_{avg}(X)$ (to maximize average torque), $f_2(X) = \Delta T_r(X)$ (to minimize torque ripple), $w_1 = w_2 = 0.5$ to ensure equal weighting between objectives.

The torque ripple ΔT_r is defined as:

$$\Delta T_r = \frac{T_{\max} - T_{\min}}{T_{avg}} \times 100\%, \quad (6)$$

where T_{max} and T_{min} are the peak and minimum torque values, respectively.

The optimization problem considers five critical design variables, which influence the electromagnetic performance of the WFFSM:

$$X = [D_{out}, l_s, g, N_{AC}, N_{DC}], \quad (7)$$

The design limits are outlined in Table 2, ensuring safe and efficient operation in industrial applications.

Table 2: Limits of design variables

Symbol	Lower Bound	Upper Bound
D_{out} (mm)	168.28	205.68
l_s (mm)	50.40	61.60
g (mm)	0.90	1.10
N_{AC}	129	159
N_{DC}	129	159

To efficiently explore the design space and reduce the computational expense of direct FEA-based optimization, a surrogate model using RSM is developed. The relationship between the design variables and the objective functions is modeled using a second-order polynomial function, which provides an accurate yet computationally efficient representation [7], [19]:

$$Y = \beta_0 + \sum_{i=1}^{n} \beta_i X_i + \sum_{i=1}^{n} \beta_{ii} X_i^2 + \sum_{i=1}^{n} \sum_{j=1}^{n} \beta_{ij} X_i X_j + \varepsilon, \quad (8)$$

where Y represents the objective function (T_{avg} or ΔT_r), X_i are the design variables influencing machine performance, β_0 is the intercept, β_i are the linear regression coefficients representing the first-order effects of the design variables, β_{ii} are the quadratic coefficients that model the nonlinear response of the system, β_{ij} are the interaction terms that capture the coupling effects between different design variables, and ε is the error term that accounts for unexplained variance in the response. A least squares approximation is used to train the model, ensuring a high coefficient of determination ($R^2 \geq 0.98$).

This quadratic response surface equation enables rapid evaluation of machine performance for different design configurations, without requiring time-consuming FEA simulations.

4.0 RESULTS AND DISCUSSION

This section presents a comprehensive evaluation of the proposed design methodology by analyzing the optimization outcomes, electromagnetic characteristics, and performance comparisons of the initial, parameterized, and optimized models. The analysis is conducted through key performance indicators such as back-EMF, flux linkage, torque characteristics, and optimization trends. Similar multi-objective optimization strategies have been successfully applied in recent industrial automation studies [20].

Figures 3 and 4 illustrate the influence of key design parameters on the T_{avg} and T_r of the WFFSM, respectively. These response surface plots provide valuable insights into the relationships between critical machine parameters.

Figure 3(a) illustrates that increasing both the air gap and the number of armature turns enhances average torque. A greater number of turns strengthen the magnetic field, leading to improved torque performance. Although a larger air gap generally reduces magnetic coupling, in this case a moderate increase in air gap improves mechanical tolerances and reduces localized flux saturation, enabling more uniform flux paths and smoother torque characteristics, as observed in Figure 3(a). Similarly, Figure 3(b) shows that reducing the stator outer diameter enhances flux concentration, which in turn contributes to better torque generation. Furthermore, Figure 3(c) reveals that increasing the number of field winding turns strengthens the excitation field, further amplifying torque output. Comparing Figures 3(a) and 3(c), it is observed that increasing the number of armature turns in conjunction with air gap length primarily enhances the magnetic motive force in the armature windings, which directly contributes to torque production. In contrast, increasing field winding turns with air gap influences the excitation flux more substantially, providing an indirect

enhancement of torque through improved flux coupling. Thus, both strategies contribute to torque improvement via different mechanisms.

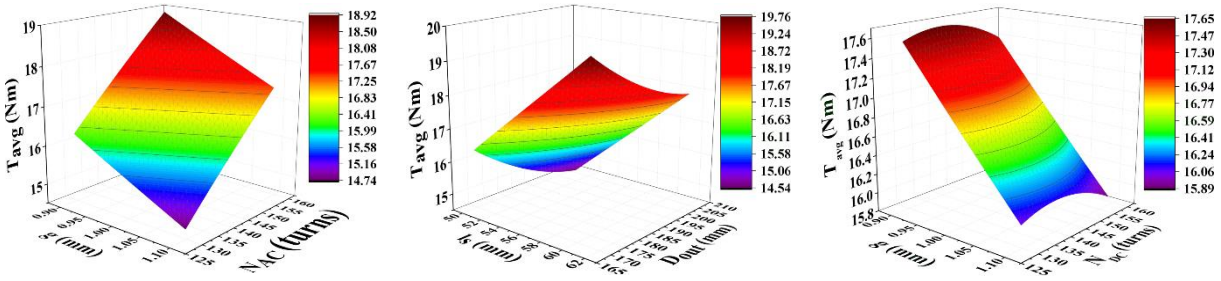

(a) (b) (c)

Figure 3: Response surface plots illustrating the influence of key design parameters on average torque: (a) g vs. N_{AC}, (b) l_s vs. D_{out}, and (c) g vs. N_{DC}

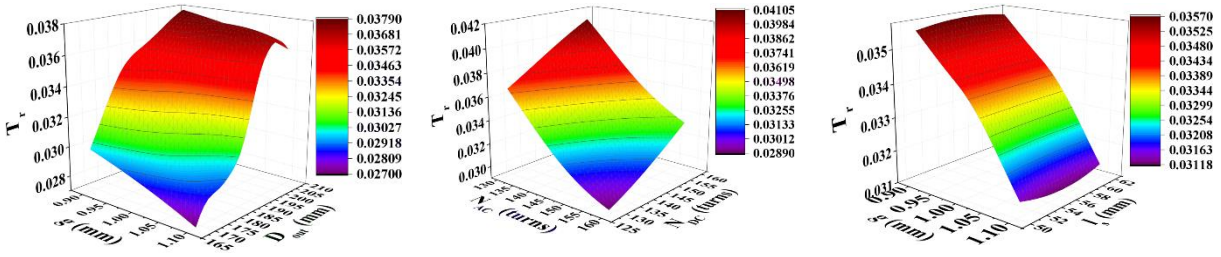

(a) (b) (c)

Figure 4: Response surface plots illustrating the influence of key design parameters on torque ripple: (a) g vs. D_{out}, (b) N_{AC} vs. N_{DC}, and (c) g vs. l_s

Building on these insights, Figure 4(a) demonstrates that increasing the air gap not only influences torque but also helps reduce torque ripple by minimizing slotting effects. Additionally, Figure 4(b) highlights that optimizing both the number of armature and field winding turns simultaneously contributes to a significant reduction in torque ripple. The simultaneous optimization of both armature and field winding turns in Figure 4(b) enables more balanced flux distribution across the stator teeth, reducing harmonic content and torque ripple. Moreover, the optimized number of turns works synergistically with the increased air gap length to stabilize the flux paths, further enhancing ripple suppression. Lastly, Figure 4(c) suggests that the stator stack length plays a crucial role in stabilizing torque output by mitigating oscillations, further enhancing the overall electromagnetic performance of the machine.

Figure 5 illustrates the Pareto front of feasible solutions, depicting the trade-off between T_{avg} and T_r. The solutions are color-coded, with the highest-ranked solutions marked in red, while the least favorable are in blue. Among the candidates, Solution II emerges as the most optimal design, balancing high torque with minimal torque ripple. Consequently, this solution is selected for comparative analysis against the initial and parameterized models.

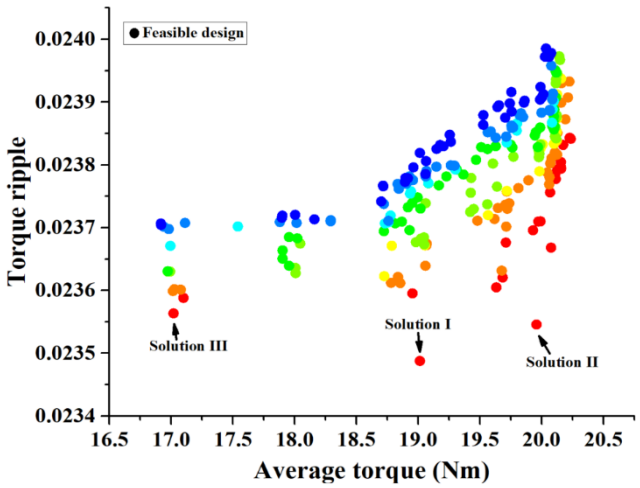

Figure 5: Pareto front of feasible solutions illustrating the trade-off between T_{avg} and T_r

Table 3: Key Design Parameters for the Candidate Solutions.

Parameter	Solution I	Solution II (Optimal)	Solution III
g (mm)	1.0980	1.0951	1.0984
D_{out} (mm)	168.52	168.57	168.52
l_s (mm)	57.88	60.89	51.23
N_{AC} (turns)	158	158	158
N_{DC} (turns)	130	130	130
T_{avg} (Nm)	19.013	19.958 (Optimal)	17.019

T_r	0.023488	0.023546	0.023564

A detailed summary of the candidate points is presented in Table 3, where key design parameters such as g, D_{out}, l_s, and N_{AC} and N_{DC} are compared. The optimal design (Solution II) exhibits the highest torque of 19.958 Nm while maintaining a low torque ripple of 0.023546.

Figures 6, 7, and 8 illustrate the magnetic density distribution and flux lines for the initial, parameterized, and optimized models under no-load and on-load conditions.

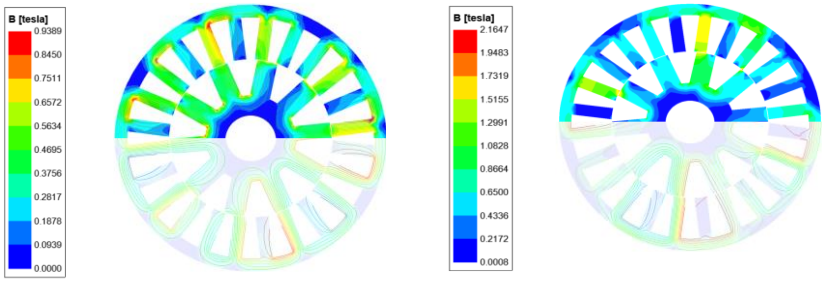

(a) (b)

Figure 6: Magnetic density distribution and flux lines of the initial model under different operating conditions: (a) No-load state, (b) On-load state

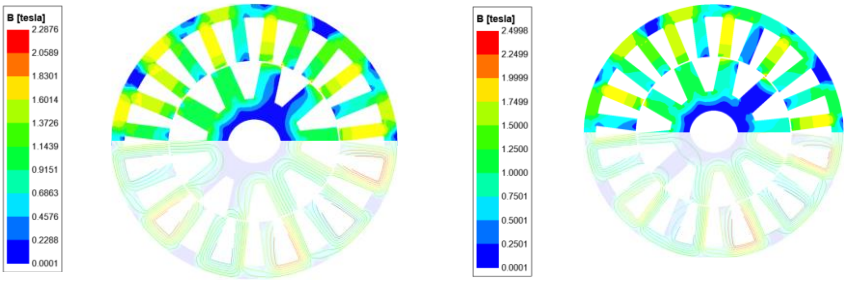

(a) (b)

Figure 7: Magnetic density distribution and flux lines of the parameterized model under different operating conditions: (a) No-load state, (b) On-load state

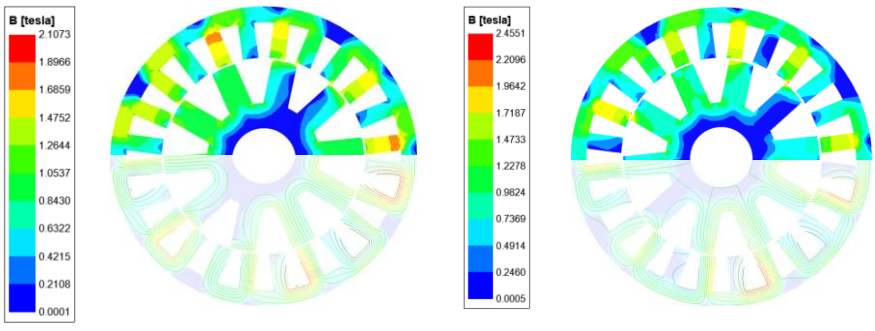

(a) (b)

Figure 8: Magnetic density distribution and flux lines of the optimized model under different operating conditions: (a) No-load state, (b) On-load state

As observed in Figure 6, the initial model exhibits weaker flux concentration due to suboptimal stator and rotor design, leading to non-uniform flux distribution. In Figure 7, the parameterized model demonstrates moderate improvements, achieving better flux uniformity than the initial model but still displaying flux leakage in certain regions. The optimized model, shown in Figure 8, achieves the most uniform flux distribution, reducing localized saturation. This improved flux behavior results in higher peak flux density in critical regions, correlating with enhanced electromagnetic torque capability compared to the other models

Figure 9 presents the comparison of the back-EMF waveforms for the three models.

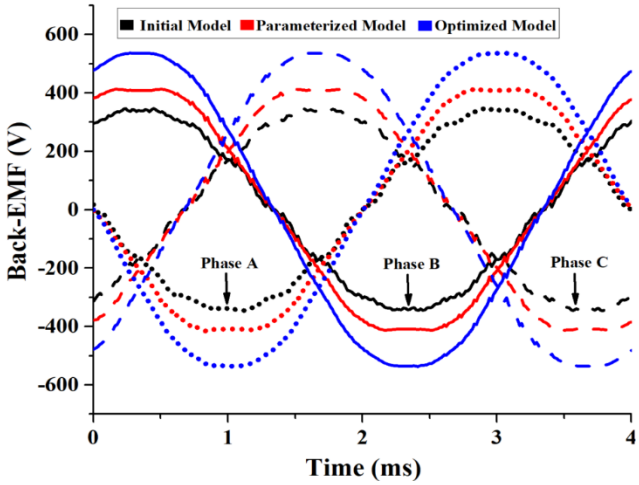

Figure 9: Comparison of Back-EMF waveforms for the initial, parameterized, and optimized models

The optimized model of Figure 9 exhibits the highest back-EMF amplitude (~365V), correlating with its enhanced torque capability. The parameterized model achieves an intermediate back-EMF (~301V), reflecting its improved but unoptimized excitation. In contrast, the initial model records the lowest back-EMF (~243V) due to its lower excitation current and weaker flux linkage.

Figure 10 compares the flux linkage waveforms under no-load conditions.

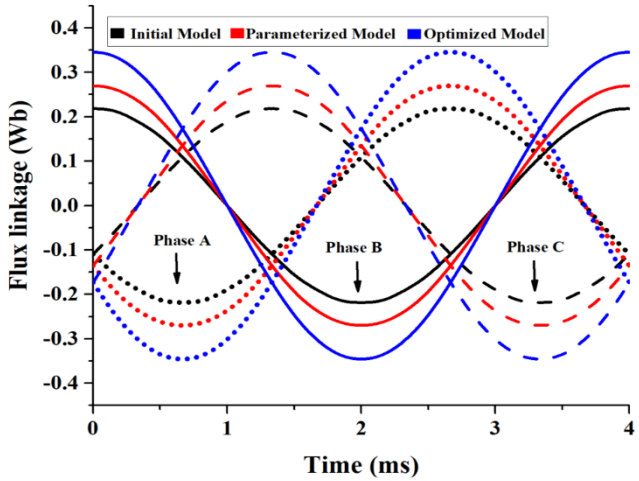

Figure 10: Flux linkage waveforms of the initial, parameterized, and optimized models at no-load operation

The optimized model attains the highest flux linkage (~0.38 Wb), attributed to its enhanced stator and rotor configuration, which strengthens the excitation field (Figure 10). The parameterized model achieves an intermediate flux linkage of ~0.30 Wb, while the initial model records the lowest value at ~0.27 Wb, reflecting its suboptimal magnetic path. Additionally, the optimized model exhibits improved phase symmetry, ensuring a more balanced torque output, whereas the initial model shows slight asymmetries, which may contribute to torque fluctuations.

Table 4 summarizes the key parameters derived from the back-EMF and flux linkage analysis.

Table 4: Comparison of back-EMF and flux linkage characteristics

Model	Peak Back-EMF (V)	RMS Back-EMF (V)	Flux linkage (Wb)
Initial Model	243.60	172.40	0.277
Parameterized Model	301.40	215.20	0.319
Optimized Model	365.30	261.60	0.385

Figure 11 illustrates the electromagnetic torque waveforms. The optimized model achieves the highest average torque (T_{avg} = 19.96 Nm), confirming the effectiveness of the optimization. The parameterized model records 16.86 Nm, while the initial model reaches only 9.77 Nm. The torque ripple for the optimized model is significantly reduced to 2.35%, compared to 10.56% in the initial model and 3.4% in the parameterized model. This substantial reduction in torque ripple signifies improved operational smoothness, leading to lower vibrations and noise, which is crucial for stable and efficient machine performance.

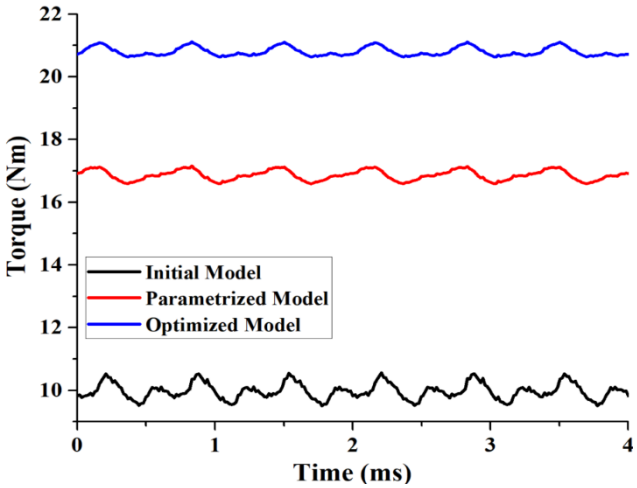

Figure 11: Electromagnetic torque characteristics of the initial, parameterized, and optimized models

A detailed comparison of key performance indicators is presented in Table 5.

Table 5: Comparative Analysis of WFFSM Models.

Parameter	Initial Model	Parameterized Model	Optimized Model
g (mm)	0.50	1.00	1.10
D_{out} (mm)	186.98	186.98	168.57
l_s (mm)	78.53	56	60.88
N_{AC} (turns)	144	144	158
N_{DC} (turns)	144	144	130
T_{avg} (Nm)	9.77	16.86	19.96

T_r (%)	10.56	3.40	2.35
T/A (Nm/A)	0.07	0.12	0.13
Back-EMF RMS (V)	243	301	365
Flux linkage (Wb)	0.27	0.30	0.38

The comparative analysis in Table 5 highlights significant performance improvements in the optimized model. The stator outer diameter was reduced by 9.85%, enhancing flux concentration for better electromagnetic performance. Armature turns increased by 9.6%, while field winding turns decreased by 9.9%, ensuring a balance between excitation and saturation. Average torque more than doubled, rising from 9.77 Nm to 19.96 Nm, while torque ripple dropped by 77.7% (from 10.56% to 2.35%), resulting in smoother operation. The torque per ampere (T/A) ratio improved from 0.06785 Nm/A in the initial model to 0.1264 Nm/A in the optimized model, confirming that performance gains were driven by design enhancements rather than increased excitation alone. Additionally, back-EMF increased by 50.2%, and flux linkage improved by 40.7%, validating the optimization strategy in boosting WFFSM efficiency and electromagnetic performance.

5.0 CONCLUSION

This study presented a comprehensive optimization framework for the WFFSM using RSM and MOGA. The proposed approach successfully improved key performance metrics, demonstrating the effectiveness of parameter tuning in enhancing machine characteristics. Comparative analysis between the initial, parameterized, and optimized models revealed substantial improvements in electromagnetic performance.

Key findings indicate that the optimized model achieved a 104.3% increase in average torque, a 77.7% reduction in torque ripple, and a 50.2% enhancement in back-EMF. The increase in air gap length and optimized stator dimensions facilitated better flux concentration, while the strategic adjustment of armature and field winding turns ensured an optimal trade-off between excitation and saturation. Furthermore, the flux linkage improved by 40.7%, reflecting enhanced electromagnetic coupling. The results validate the effectiveness of the surrogate-based optimization strategy in achieving high torque density and reduced torque ripple. The optimized WFFSM exhibits superior electromagnetic performance, making it a promising candidate for high-performance industrial applications. Future work will consider more robust multi-objective and multi-variable optimization approaches, integrating additional design constraints and efficiency metrics to further refine the machine's performance. Additionally, experimental validation of the optimized design will be conducted to verify the computational results and assess the practical feasibility of the proposed methodology.

6.0 ACKNOWLEDGEMENT

This work is supported by 2020 TEFTUND National Research Grant Intervention (Grant No. NRF/SETI/III/00055).

REFERENCES

[1] Guo, Y., Lin, L., Xin, B., Haiyan, L., Gang, L., Wenliang, Y., and Jianguo, Z. "Designing high-power-density electric motors for electric vehicles with advanced magnetic materials." *World Electric Vehicle Journal*, vol. 14, no. 4, 114, 2023. doi:10.3390/wevj14040114.

[2] Akuru, U. B., Mkhululi, M., and Maarten, J. K. "On the electromagnetic performance prediction of turbo synchronous condensers based on wound-field flux switching machine design." *IEEE Transactions on Industry Applications*, vol. 57, no. 4, pp. 3687-3698, 2021. doi: 10.1109/TIA.2021.3080668.

[3] Abunike, C. E., Akuru, U. B., Okoro, O.I. and Awah, C. C. "Sizing, modeling, and performance comparison of squirrel-cage induction and wound-field flux switching motors." *Mathematics*, vol. 11, no. 16, 3596, 2023. doi: 10.3390/math11163596.

[4] Akuru, U. B., and Maarten, J. K. "Formulation and multiobjective design optimization of wound-field flux switching machines for wind energy drives." *IEEE Transactions on Industrial Electronics*, vol. 65, no. 2, pp. 1828-1836, 2017. doi: 10.1109/TIE.2017.2721928.

[5] Aminu, M. "A parameter estimation algorithm for induction machines using artificial bee colony optimization." *Nigerian Journal of Technology*, vol. 38, no. 1, pp. 193-201, 2019. doi: 10.4314/njt.v38i1.24.

[6] Abunike, C. E., Okoro, O. I., Aliakbar, J. F., and Aphale, S. S. "Advancements in flux switching machine optimization: Applications and future prospects." *IEEE Access*, vol. 11, pp. 110910-110942, 2023. doi:10.1109/ACCESS.2023.3321862.

[7] Cheng, M., Zhao, X., Dhimish, M., Qiu, W. and Niu, S. "A Review of Data-Driven Surrogate Models for Design Optimization of Electric Motors," *IEEE Transactions on Transportation Electrification*, vol. 10, no. 4, pp. 8413-8431, Dec. 2024. doi: 10.1109/TTE.2024.3366417.

[8] Orosz, T., Anton, R., Ants, K., Pedro, A., David, P., Jan, K., and Pavel, K. "Robust design optimization and emerging technologies for electrical machines: Challenges and open problems." *Applied Sciences*, vol. 10, no. 19, 6653, 2020. doi: 10.3390/app10196653

[9] Meng, Y., Fang, S., Zhu, Y., Chen, H., Zhong, Y., and Qin, L. "Surrogate-Model-Based Multilevel Optimization Design and Analysis of a New Flux Switching Machine With Double-Sided PM Excitation," *IEEE Transactions on Transportation Electrification*, vol. 10, no. 4, pp. 10136-10146, 2024. doi: 10.1109/TTE.2024.3358392

[10] Du, Y., Gu, J., Zhang, H. and Hua, W. "Reliability-Based Robust Optimization of High-Speed PM Synchronous Machine With Local Surrogate Model Strategy", *IEEE Transactions on Transportation Electrification*, vol. 10, no. 4, pp.9679-9690, 2024. doi: 10.1109/TTE.2024.3360112

[11] Yang, Y., Zhang, C., Bramerdorfer, G., Bianchi, N., Qu, J., Zhao, J. and Zhang, S. "A computationally efficient surrogate model based robust optimization for permanent magnet synchronous machines", *IEEE Transactions on Energy Conversion*, vol. 37, no. 3, pp.1520-1532, 2022. doi: 10.1109/TEC. 2021.3140096

[12] Qin, Q. H., Yu, S. F., Qiongfang, Z., and Yulei, L. "Hybrid Surrogate Model based Multi-objective Optimization Design of Flux-Modulated Permanent Magnet Machine for Shaftless Pump-Jet Propulsor." *IEEE Transactions on Magnetics*, vol. 60, no. 12, pp. 1-5, 2024. doi: 10.1109/TMAG.2024.3476247

[13] Zhang, W., Wu, Z., Jin, L., Fan, Y., Hua, W., and Cheng, M. "Analysis and Multi-Objective Optimization of the Hybrid Excitation Switched Flux Machine," *IEEE Transactions on Industry Applications*, vol. 1, no. 11, pp. 1-11, 2025. doi: 10.1109/TIA.2025.3532244

[14] Xu, Z., Cheng, M., Wen, H., and Jiang, Y. "Design and Many-Objective Optimization of an In-Wheel Hybrid-Excitation Flux-Switching Machine Based on the Kriging Model," *IEEE Transactions on Transportation Electrification*, vol. 11, no. 1, pp. 2368-2379, 2025. doi: 10.1109/TTE.2024.3422290

[15] Ghafariasl, P., Alireza, M., Mahmoud, M., Aria, N., Siamak, H., Mani, F., Shing, C., Masoomeh, Z., and Davide, A. G. "Neural network-based surrogate modeling and optimization of a multigeneration system." *Applied Energy*, vol. 364, pp. 1-18, 2024. doi: 10.1016/j.apenergy.2024.123130

[16] Hu, Y., Zhang, W., Zhang, Y., Xu, W. and Wang, J. "Surrogate-Assisted Adaptive Design Optimization of Magnetorheological Fluid Brake-Integrated AFPM Machine with Different Brake Torque Ratios," *IEEE Transactions on Energy Conversion*, vol. 1, no. 14, 2025. doi: 10.1109/TEC.2025.3543312

[17] Guo, S., Su, X. and Zhao, H. "Optimal Design of an Interior Permanent Magnet Synchronous Motor for Electric Vehicle Applications Using a Machine Learning-Based Surrogate Model", *Energies*, vol. 17, no. 16, pp. 3864, 2024. doi: 10.3390/en17163864

[18] Guo, S., Xiangdong, S., and Hang, Z. "Optimal Design of an Interior Permanent Magnet Synchronous Motor for Electric Vehicle Applications Using a Machine Learning-Based Surrogate Model." *Energies*, vol. 17, no. 16, 3864, 2024. doi: 10.3390/en17163864

[19] Ling, C., Kuo, W. and Xie, M. "An overview of adaptive-surrogate-model-assisted methods for reliability-based design optimization", *IEEE Transactions on Reliability*, vol. 72, no. 3, pp.1243-1264, 2022. doi: 10.1109/TR.2022.3200137

[20] Gong, Y., Gneiting, A., Weigel, S., Parspour, N., and An, Z. "Surrogate Model Based Drive Cycle Modelling and Optimization of Synchronous Reluctance Machines for Electric Vehicles", *IEEE Transactions on Magnetics*, vol. 6, no. 1, pp. 1-5, 2025. doi: 10.1109/TMAG.2025.3544386